Journal of Neuroscience Methods 406 (2024) 110137

Contents lists available at ScienceDirect

Journal of Neuroscience Methods

journal homepage: www.elsevier.com/locate/jneumeth

Simultaneous isolation of intact brain cells and cell-specific extracellular vesicles from cryopreserved Alzheimer's disease cortex

Mikhail Melnik [a,d], Emily Miyoshi [a], Ricky Ma [a], Maria Corrada [f,h], Claudia Kawas [f,g,h], Ryan Bohannan [h], Chad Caraway [h], Carol A. Miller [e], Jason D. Hinman [b,c], Varghese John [b,c], Tina Bilousova [a,b,c,*], Karen H. Gylys [a,b,d]

[a] UCLA School of Nursing, Los Angeles, CA 90095, USA
[b] Mary S. Easton Center for Alzheimer's Research at UCLA, Los Angeles, CA 90073, USA
[c] Departments of Neurology, UCLA School of Medicine, Los Angeles, CA 90095, USA
[d] Neuroscience Interdepartmental Program, UCLA School of Medicine, Los Angeles, CA 90095, USA
[e] Keck USC School of Medicine, Los Angeles, CA 90033, USA
[f] Departments of Neurology, Irvine, CA 92697, USA
[g] Neurobiology & Behavior, Irvine, CA 92697, USA
[h] Institute for Memory Impairments and Neurological Disorders, UC Irvine, Irvine, CA 92697, USA

ARTICLE INFO

Keywords:
Flow cytometry
Dissociation
Neurons
Microglia
Astrocytes
Oligodendrocytes
Extracellular vesicles
Exosomes

ABSTRACT

Background: The neuronal and gliaI populations within the brain are tightly interwoven, making isolation and study of large populations of a single cell type from brain tissue a major technical challenge. Concurrently, cell-type specific extracellular vesicles (EVs) hold enormous diagnostic and therapeutic potential in neurodegenerative disorders including Alzheimer's disease (AD).

New method: Postmortem AD cortical samples were thawed and gently dissociated. Following filtration, myelin and red blood cell removal, cell pellets were immunolabeled with fluorescent antibodies and analyzed by flow cytometry. The cell pellet supernatant was applied to a triple sucrose cushion for brain EV isolation.

Results: Neuronal, astrocyte and microglial cell populations were identified. Cell integrity was demonstrated using calcein AM, which is retained by cells with esterase activity and an intact membrane. For some experiments cell pellets were fixed, permeabilized, and immunolabeled for cell-specific markers. Characterization of brain small EV fractions showed the expected size, depletion of EV negative markers, and enrichment in positive and cell-type specific markers.

Comparison with existing methods and conclusions: We optimized and integrated established protocols, aiming to maximize information obtained from each human autopsy brain sample. The uniqueness of our method lies in its capability to isolate cells and EVs from a single cryopreserved brain sample. Our results not only demonstrate the feasibility of isolating specific brain cell subpopulations for RNA-seq but also validate these subpopulations at the protein level. The accelerated study of EVs from human samples is crucial for a better understanding of their contribution to neuron/glial crosstalk and disease progression.

1. Introduction

Based on advances in cell transcriptomic techniques, the last 5–10 years have seen an enormous surge of studies focused on microglial subtypes in a number of acute and chronic neurologic diseases that include traumatic brain injury and Alzheimer's disease (AD). Importantly, cell-specific transcriptomics are relevant for study of all brain cell populations including neurons, astrocytes, endothelial cells, and oligodendrocytes, always with the requirement of obtaining a pure subtype population, generally using flow cytometry or laser microdissection. As a key example, a number of AD-specific microglial subpopulations have been identified that include disease associated microglia (DAM) (Keren-Shaul et al., 2017), *APOE*-driven neurodegenerative microglia (Krasemann et al., 2017), and dark microglia (Bisht et al., 2016). Other papers show specific phenotypic changes associated with astrocytes in Alzheimer's, including induction of A1 astrocytes

* Correspondence to: Department of Physiological Nursing, UCSF School of Nursing, 2 Koret Way, N713, USA.
E-mail address: tina.bilousova@ucsf.edu (T. Bilousova).

https://doi.org/10.1016/j.jneumeth.2024.110137
Received 15 December 2023; Received in revised form 25 March 2024; Accepted 12 April 2024
Available online 14 April 2024

(Liddelow et al., 2017), disease-associated astrocytes (DAAs) as well as others, including interferon-positive astrocytes (Hasel et al., 2021; Mathys et al., 2019). There was also evidence of astrocytic phenotypes that were maintained in control and AD brain but showed underlying gene expression changes (Sadick et al., 2022). However, recent guidelines emphasize that labeling of astrocytes and microglial states oversimplifies the complicated physiologic responsiveness of both cell types and should be avoided (Escartin et al., 2021). However, much of the data on phenotypes is based on RNA sequencing (RNAseq) changes, not proteomic changes, likely more accurate reflections of function, and functional loss, in AD cell subtypes. Furthermore, much of the RNAseq data which was used to find particular microglial and astrocytic phenotypes was performed in mouse models of AD and either does not replicate or shows lower overlap with human phenotypes (Grubman et al., 2021; Mathys et al., 2019; Zhou et al., 2020). This may be due to the inherent weaknesses of AD mouse models (e.g. lack of neurofibrillary tangles) as well as agonal state and post-mortem interval effects on human brain tissue.

Small extracellular vesicles (EVs) are a separate topic of great interest across disciplines from cancer biology to neurodegeneration, although almost nothing is known about the pathological functions of different brain extracellular vesicles. Small EVs is an umbrella term encompassing nanoscale vesicles (30–200 nm) of various origins, which include small-size ectosomes, derived from plasma membrane, and exosomes, a subset of small EVs derived from multivesicular bodies (Buss et al., 2021; Rastogi et al., 2021; Welsh et al., 2024). They carry as cargos a number of specific proteins, lipids, and microRNAs (miRNAs), and have a number of cell signaling functions, including spread of neuroinflammation and misfolded proteins, particularly tau, in neurodegeneration (Asai et al., 2015; Fernandes et al., 2018; Gao et al., 2019; Guix et al., 2018; Kaufman et al., 2017; Polanco et al., 2016). Recent studies have also focused on the enormous potential of small EVs, as diagnostic biomarkers with potential therapeutic applications (Buss et al., 2021; Rastogi et al., 2021), particularly for Alzheimer's disease. EVs can be isolated by size using ultracentrifugation and size exclusion chromatography (SEC), and can also be isolated by precipitation, immunocapture, ultrafiltration, field-flow fractionation, and microfluidics, or a combination of methods (Stam et al., 2021).

Transcriptomic approaches have exploded in recent years but complex tissues like brain require dissociation, and the subsequent rapid decline of cell and RNA quality has generally necessitated use of animal models or immediately postmortem or postoperative human samples (Olah et al., 2020), a great constraint on experimental design. Cryopreservation prevents the formation of ice crystals and is routinely used to bank immortalized cell lines for tissue culture, and has been used to isolate neural stem cells from human biopsy samples that are equally viable to those from fresh tissue (Palmero et al., 2016). We and a number of other labs routinely bank cryopreserved human postmortem tissue in order to use the synaptosome model system of resealed nerve terminals (Ahmad and Liu, 2020). With the goal of making isolation of brain cell types possible with banked tissue, at the same time maximizing individual samples by allowing cell-specific small EV isolation from the same samples, we have developed a protocol for simultaneous isolation of cells and small EVs from cryopreserved human postmortem samples.

2. Materials and methods

2.1. Materials

Directly-labeled antibodies, except for those targeting myelin basic protein (MBP), were used for fluorescent labeling of cells in dissociation experiments. The Zenon isotype-specific labeling kit (Thermo Fisher Scientific, Rockville, IL) was utilized according to the manufacturer's instructions to fluorescently label MBP antibodies. Fluorophores were carefully chosen for each experiment to prevent spectral overlap and the need for compensation in flow cytometry experiments. Table 1 lists all the antibodies employed for flow cytometry, immunoprecipitation, and immunoblotting analyses in the paper. Isotype control antibodies were utilized to determine non-specific binding.

Table 1
List of antibodies used for flow cytometry, immunoprecipitation and immunoblotting analysis.

Antibody target (Fluorophore)	Manufacturer / Catalog #
CD63	Thermo Fisher / 10628D
CD9	Thermo Fisher / 10626D
ALIX	Santa Cruz Biotech / sc-99010
Syntenin-1	Santa Cruz Biotech / sc-515538
GM130	Cell Signaling Tech / 12,480 T
Calnexin	Santa Cruz Biotech / sc-23964
CD171 / L1CAM	Thermo Fisher / MA1–46044
Isotype control for CD171	BioLegend / 400,102
CD11b	BioLegend / 101,214
Isotype control for CD11b	BioLegend / 400,622
GLAST / ACSA-1	Miltenyi Biotec / 130–095–822
Isotype control for GLAST	BioLegend / 401,502
MOG	Santa Cruz Biotech / sc-166172
CD56 (PE-Vio770)	Miltenyi Biotec / 130–113–870
NeuN (Alexa fluor 674)	Abcam/ ab190565
CD11b (VioBlue)	Miltenyi Biotec / 130–110–558
GFAP (PE)	Miltenyi Biotec / 130–105–329
TGF-β (VioBright FITC)	Miltenyi Biotec / 130–106–994
O4 (APC)	Miltenyi Biotec / 130–119–155
MBP (Zenon: Alexa fluor 488)	Calbiochem / NE1018
Isotype control for MBP (Zenon: Alexa fluor 488)	Biolegend/ 400,102

2.2. Cryopreservation of human samples

Human AD cortical samples, generally from 1 to 2 g, were prepared as described in (Gylys and Bilousova, 2017); for dissociation experiments, only cases with PMI $\leq$ 6 h were used. Briefly, following harvesting of human brain from Brodmann areas A7, A9, A39 or A40, tissue was finely minced (1–3 mm fragments) on ice and suspended in a solution of sucrose and protease inhibitors (0.32 M sucrose, 2 mM EDTA, 2 mM EGTA, 0.2 mM PMSF, 1 mM NaPP, 5 mM NaF, 10 mM Tris-HCl, pH 8.0), with 10 mL sucrose buffer/g tissue, and then slowly frozen to –80 °C; this protocol is based on a previous optimization (Dodd et al., 1986). For certain experiments, minced tissue samples were kept in commercial Hibernate media (Gibco, Thermo Fisher Scientific, Rockville, IL) for a brief duration instead of undergoing immediate cryopreservation. Detailed information for all cases used in the paper are

Table 2
Case information for human samples.

Case	Sex	Age	PMI (h)	Braak Stage	Plaque Stage	Figures used from Cases
AD 1	M	87	5.5	V-VI	B	Fig. 2A
AD 2	M	89	4.25	V	C	Fig. 2B - D
AD 3	F	93	5.58	V	C	Fig. 3
AD 4	F	92	4.75	VI	C	Fig. 4A-D
CTL 1	F	65	6	I	0	Fig. 4A-D
AD 5	F	87	6.03	VI	C	Fig. 4C and D
AD 6	F	95	6.2	VI	C	Fig. 4C and D
AD 7	M	88	6.55	VI	C	Fig. 4C and D
AD 8	M	86	4.83	V	B	Fig. 4C and D
AD 9	M	95	4.83	V	B	Fig. 4C and D
AD 10	F	73	5.75	VI	C	Fig. 4C and D
AD 11	F	91	4.38	VI	B	Fig. 4C and D
AD 12	F	55	5.57	VI	B	Fig. 4C and D
AD 13	F	90	6.33	VI	B	Fig. 4C and D
CTL 2	F	91	6.85	II	0	Fig. 4C and D
CTL 3	F	100	3.75	III	0	Fig. 4C and D

listed in Table 2.

2.3. Cell dissociation

Cryopreserved human AD and control brain samples were quickly defrosted at 37 °C, centrifuged at 1000xg for 2 min at 4 °C to remove cryopreservation buffer. Cell suspensions were processed for 30 min at 37 °C using a brain dissociation kit either with papain or with trypsin and the gentleMACS Octo dissociator (all three from Miltenyi Biotec, San Diego, CA), according to manufacturer's instructions. The Papain kit yielded the highest number of live cells in a recent paper comparing six different enzyme protocols for cell dissociation from rodent brain (Hussain et al., 2018), but some surface proteins, for example astrocytic marker glutamate aspartate transporter (GLAST) (Kantzer et al., 2017), are sensitive to papain treatment, thus the dissociation method was chosen based on the downstream analysis. Following dissociation, the single-cell suspension was passed through MACS SmartStrainers (70 μm; Miltenyi Biotec, San Diego, CA) and then centrifuged at 300 x *g* for 10 minutes at 4 °C, followed by myelin removal and red blood cell (RBC) removal per kit instructions. A small amount of cell pellet after the first centrifugation was supplemented with protease and phosphatase inhibitors and stored at −80 °C until homogenization. For immunolabeling, purified brain cells were first incubated with antibodies for cell surface markers (e.g., CD11b), then fixed and permeabilized prior to incubation with antibodies to intracellular proteins (e.g. NeuN). Labeled cells were analyzed by flow cytometry using an LSRII cytometer (Becton Dickinson, Franklin Lakes, NJ) and FCS Express software version 5 (DeNovo Software, Pasadena, CA). Two types of data were recorded for each marker: the percentage of intact cells that labeled for the marker (i.e. positive population) and the intensity of marker labeling within the positive population, measured in relative fluorescence units (RFU).

2.4. Isolation of brain-derived EVs

The supernatant was centrifuged at 2000 x *g* for 10 min at 4 °C, and then the resulting supernatant was collected and subjected to centrifugation at 10,000 x *g* for 30 min at 4 °C. The supernatant obtained from the last centrifugation step was layered onto a triple sucrose cushion gradient for ultracentrifugation (180,000 x *g* for 3 h, 4°C) (Vella et al., 2017). As described, Fractions 1–3 (F1–3) were collected, diluted, and subjected to a final spin (100,000 x g for 1 hour, 4°C) to pellet the vesicles. The pelleted vesicles were then suspended in 25 mM trehalose in phosphate buffered saline (PBS) to prevent aggregation and cryodamage, aliquoted, and slowly frozen at −80 °C. Before downstream analysis, sample aliquots were quickly thawed for 1 minute at 37 °C.

2.5. Transmission electron microscopy (TEM)

Samples from F1, F2, and F3 fractions were fixed on Formvar/Carbon 400 mesh, Copper TEM grids (Ted Pella, Redding, CA) using a glutaraldehyde/paraformaldehyde solution. Following fixation, they were stained with a 2 % uranyl acetate solution and imaged using a JEOL 100CX electron microscope at a magnification of 29,000x.

2.6. Tunable resistive pulse sensing analysis (TRPS)

Size distribution and concentrations of small EVs (F2) were measured by TRPS method using the qNano Gold instrument (Izon Science). NP100 nanopore (particle size range: 50–330 nm) and CPC100 calibration particles were used for the analysis. Data analysis was performed using the qNano Gold instrument software.

2.7. Immunoprecipitation of cell-specific small EVs

Antibodies, anti-CD171, anti-CD11b, anti-GLAST, and corresponding isotype control antibodies (Table 1) were covalently coupled to M-270 Epoxy Dynabeads using conjugation kit (Thermo Fisher Scientific, Rockford, IL) according to manufacturer's instructions. Small EV fraction (F2) isolated using trypsin-based tissue dissociation protocol was incubated with a human-specific FcR blocking reagent (Miltenyi Biotec, San Diego, CA) for 5 minutes, diluted 1:20 with 1 %BSA in PBS, pH 7.4, and then used for immunoprecipitation (IP). An equal amount of the diluted F2 fraction was incubated with CD171-specific Dynabeads and with corresponding isotype control-coupled beads overnight at 4 °C with rotation. After the incubation, Dynabeads with bound neuronal EVs and isotype control beads were collected using a magnet, and the remaining F2 fraction was utilized for subsequent IP reactions with anti-CD11b, anti-GLAST-coupled Dynabeads, and their corresponding isotype control-coupled Dynabeads. The incubations were carried out for 3 hours at 4°C with rotation. After the IP reaction, Dynabeads were washed with 0.1 % BSA in PBS, then with 25 mM citrate-phosphate buffer, pH 5 to reduce the amount of nonspecifically bound material as previously described (Heinzelman et al., 2016), followed by two washes with PBS, pH 7.4 (10 min at RT with rotation) and frozen at −80 °C for downstream analysis.

2.8. Western blotting

Samples were separated by non-reducing gel electrophoresis on Novex, 15 well 10–20 % Tris-Glycine gradient gels (Thermo Fisher Scientific, Rockford, IL). For marker comparison between the EV fraction and the corresponded cell fraction, the equal amount of total protein (5 μg) was loaded per lane, measured using the bicinchoninic acid (BCA) assay (Thermo Fisher Scientific, Rockford, IL). After transferring to Immobilon-P PVDF membrane (Millipore Sigma, Burlington, MA) Western blot analysis with primary antibodies (see Table 1) and corresponded secondary HRP-conjugated IgG (Jackson Immunoresearch) was performed. Immunolabeled proteins were visualized by SuperSignal West Femto maximum sensitivity substrate (Thermo Scientific, Rockford, IL). Results were obtained and quantified using a UVP BioSpectrum 600 imaging system equipped with VisionWorks Version 6.6 A software (Upland, CA).

2.9. Statistical Analysis

The Levene's test and Shapiro-Wilk test were performed to determine if the assumptions of variance homogeneity and normality of data, respectively, were observed for all groups being compared. Student's t test was performed if these two assumptions were held while a Mann-Whitney U (MWU) test was performed when the assumption of normality failed. All group comparisons showed homogeneity of variance (i.e. showed a p value greater than 0.05 for Levene's test).

3. Results

3.1. Isolation of intact brain cell types from cryopreserved samples

The major steps in the synchronized isolation of brain cells and small EVs from cryopreserved human brain tissue are illustrated in Fig. 1. After gentle enzymatic and mechanical dissociation (Step 1), removal of large undissociated debris (Step 2), and low speed centrifugation to pellet brain cells (Step 3), the supernatants used for small EV isolation, and the cell pellets underwent additional purification steps separately. Following cell debris removal (including myelin) and RBC removal steps, cells were immunolabeled and analyzed using flow cytometry.

Most brain cell dissociation studies identify a 'live cell' population that is distinct from the huge signal coming from the dead cells in the mix; this is usually illustrated with the light scattering parameters of forward scatter (FSC; proportional to size) and side scatter (SSC; related to cell granularity). Results (Fig. 2A) show the expected major population of dead cells and debris along with a smaller separate population of intact cells that have a lower SSC:FSC ratio; these plots have a similar

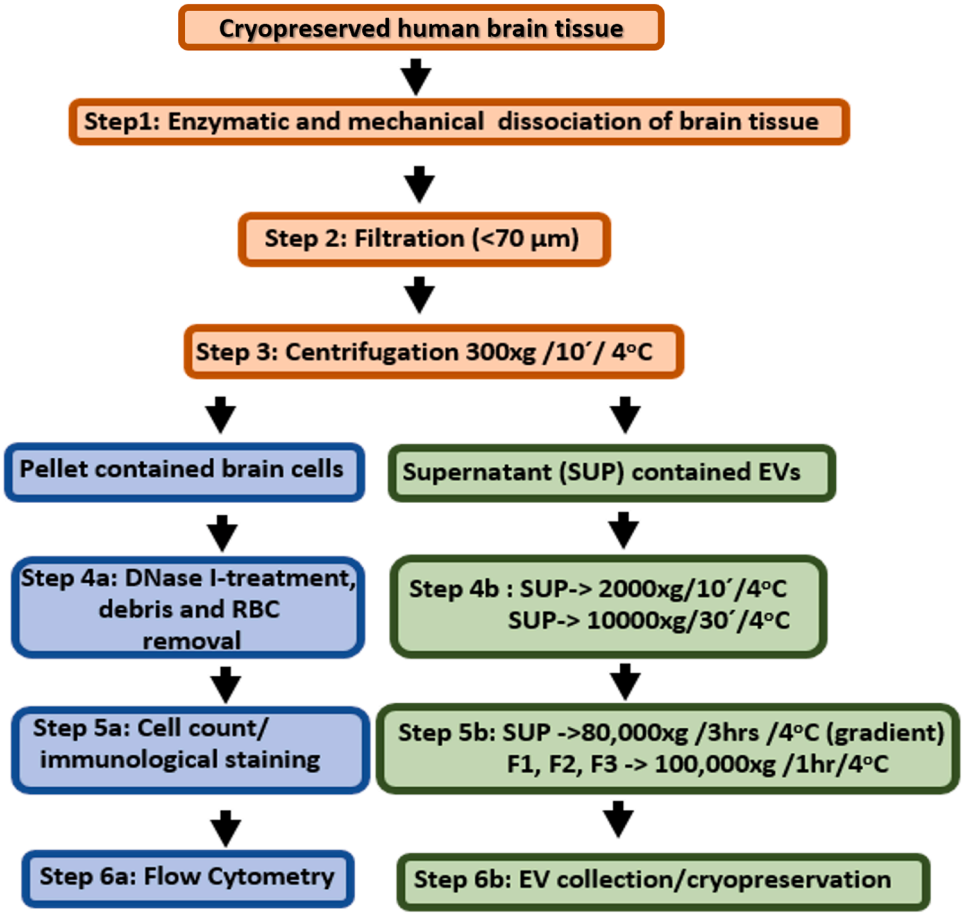

Fig. 1. Schematic flow chart for isolation of cells and cell-specific small EVs. Overview of procedural steps for cells (left) and small EVs (right).

appearance to those in the literature (Bennett et al., 2016; Srinivasan et al., 2016; Wylot et al., 2015). A similar gate drawn for intact cells is the first analytic step in each subsequent experiment. In this experiment we included a viability marker showing intact cells using calcein AM, a marker for cell viability, which labels cells with an intact membrane and esterase activity; the calcein signal was co-localized with the neuronal cell adhesion molecule (NCAM) signal (also known as CD56; Fig. 2A). For the AD sample presented in Fig. 2A, around 66 % of the intact population were calcein AM-positive, indicating that intact cells survived cryopreservation and the dissociation procedure.

3.2. Simultaneous labeling of neurons, astrocytes, and microglia from AD patient tissue

Next, we applied flow cytometry to distinguish different cell types within the intact cell population. For the experiment shown in Fig. 2B-D, three markers were used to label an AD sample: NeuN (neuronal nuclei, a neuron marker), GFAP (glial fibrillary acidic protein, an astrocyte marker), and CD11b (a marker for activated microglia). For each antibody, isotype controls demonstrate the level of background fluorescence (Fig. 2B-D, left panels). For this experiment, approximately 8 % of intact cells labeled positively for NeuN (Fig. 2 B, right), ~31 % of intact cells stained positively for GFAP (Fig. 2C, right), and ~3 % of intact cells stained positively for CD11b (Fig. 2D, right).

3.3. CD11b and TGFβ label the same population of microglia

To further characterize microglia from the intact cell population isolated from AD brain, we immunolabeled dissociated cells with two microglial markers: CD11b and transforming growth factor β1 (TGFβ1; Fig. 3A-C). CD11b is a widely used microglial marker, and TGFβ1 is a marker of homeostatic microglia that has previously been shown to be downregulated in mouse models of AD and in some other mouse models, leading to ensuing microgliosis (Butovsky et al., 2014; Krasemann et al., 2017), though transcriptomically unchanged in human AD (Mathys et al., 2019; Zhou et al., 2020).

In the AD brain tissue sample, approximately 19 % of intact cells stained positively for CD11b (Fig. 3A, right), and approximately 18 % were positive for TGFβ1 (Fig. 3B, right). The quadrant analysis showing co-localization of the CD11b and TGFβ1 signals is shown in Fig. 3C (right); ~94 % of CD11b-positive cells are co-localized with TGFβ1. Isotype controls for both antibodies are shown on the left panels.

3.4. Mature and immature oligodendrocytes in AD cortex

White matter degeneration is evident early in AD and contributes to cognitive loss; at the same time the high metabolic demand of differentiating oligodendrocyte precursor cells (OPCs) further impacts disease progression (de la Monte and Grammas, 2019; Spaas et al., 2021). To identify oligodendrocytes in our sample, we used two markers: myelin basic protein (MBP), an indicator for mature oligodendrocytes, and O4, a marker of both mature and immature oligodendrocytes. Fig. 3D-F shows flow cytometry analysis of oligodendrocytes, with MBP and O4 on the right (Figs. 3D and 3E, respectively) and the background staining for each experiment on the left. We observed that ~28 % of intact cells were positive for MBP and 5 % of intact cells were positive for O4.

The bivariate plots in Fig. 3F illustrate the co-localization of MBP and O4 signals. The majority (~23 %) of the cells label only with MBP, with ~9 % showing co-localization, reflecting the presence of mostly mature oligodendrocytes along with a small number of immature

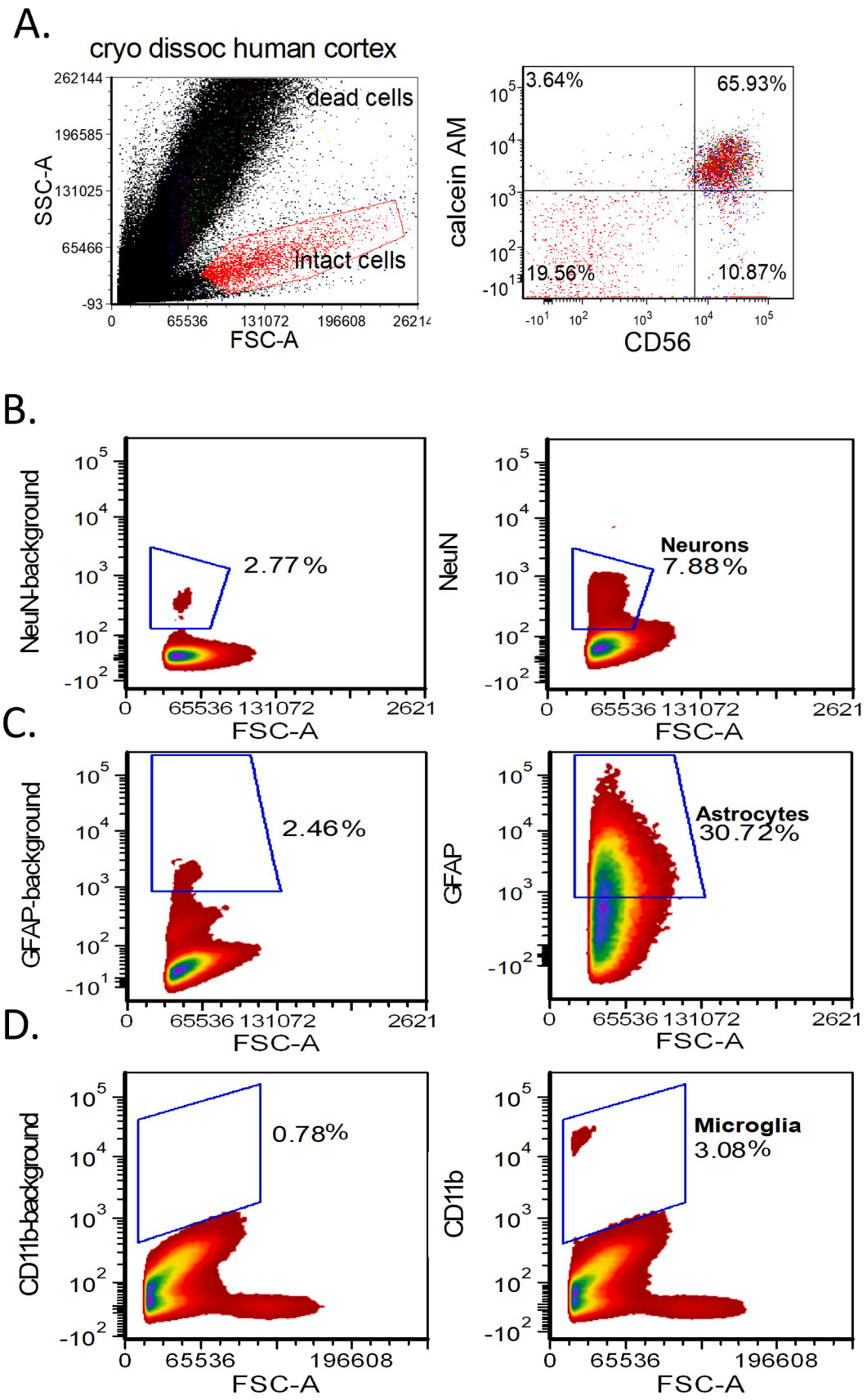

Fig. 2. Isolation of intact cells and major brain cell types from cryopreserved human cortex. (A) Light scattering parameters of forward scatter (FSC; proportional to size) and side scatter (SSC; related to cell granularity), showing the intact cell population with a lower SSC:FSC ratio (left). Calcein AM, a viability marker, labels cells with an intact membrane and esterase activity; the calcein signal was co-localized with the neuronal signal (NCAM; right). (B-D) Single sample immunolabeled for brain cell types: neuronal cell population (NeuN; B), astrocytes (GFAP, C), and microglia (CD11b, D). Background labeling is shown at left for each antibody.

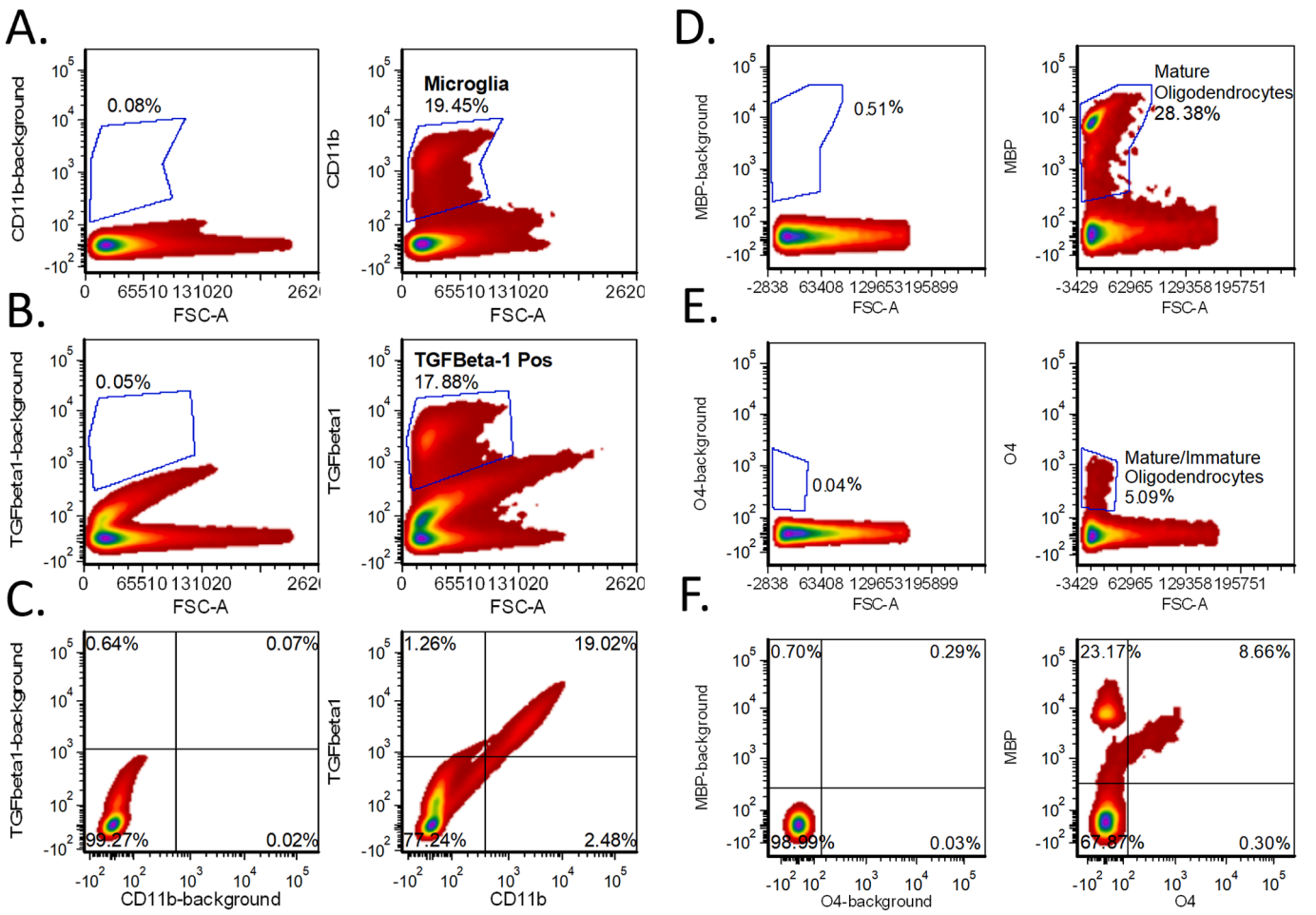

Fig. 3. Microglial and oligodendrocyte populations in human cortex. (A-C) CD11b (A) and TGFβ (B) immunolabeling of microglia is co-localized as shown in the upper right quadrant of the bivariate plot (C). Background labeling with isotype control is shown at left for each. (D-F) MBP immunolabeling of mature oligodendrocytes (D) and O4 labeling of both mature and immature oligodendrocytes (E); ~9 % of cells are dual labeled, with 23 % positive for MBP only (F). Background labeling with isotype control is shown at left for each antibody.

oligodendrocytes that express both proteins.

3.5. Comparison of CD11b-positive populations between late-stage AD and control cases

We expanded our study to include a cohort of 3 control and 10 late stage (Braak V-VI) AD cases (Table 2) and labeled them for CD11b and TGFβ1. Representative results for CD11b and TGFβ1 labeling are shown in Figs. 4A and 4B, respectively, with background staining, Control, and AD case from left to right. There were no significant differences between Control and AD groups in the percentage of CD11b- and TGFβ1-positive intact cells and their relative levels of fluorescence intensity (Fig. 4C and D).

3.6. Isolation of cell-specific small EVs

We used a combination of differential and density gradient ultracentrifugation methods (Fig. 1), which are the most widely used techniques for EV isolation (Stam et al., 2021). Similar to a number of related protocols based on an early method by Thery et al., there are five major centrifugation steps. These include two low-speed spins to remove cells, an intermediate spin at 10,000 g to eliminate cell debris, and two final ultracentrifugation steps to isolate EVs and remove contaminating proteins (Thery et al., 2006). The density gradient ultracentrifugation step in the current protocol uses a triple sucrose gradient to enrich for small EVs, assisting in their separation from proteins and reducing damage from high g-forces (Vella et al., 2017). Transmission electron microscopy (TEM) analysis of fractions 1–3 reveals that F1 contained large vesicles and membrane pieces larger than 200 nm in diameter (Fig. 5A, left). F2 exhibited an abundance of small EVs, mostly ranging in size from 50 to 200 nm (Fig. 5A, center), along with a few smaller vesicles (~10 nm). These small vesicles are likely to be high or intermediate density lipoprotein particles, which are common contaminants in EV samples (Stam et al., 2021). Fraction F3 exhibited the smallest and fewest vesicles (Fig. 5A, right). Fraction F2 was collected and characterized as the small EV fraction in accordance with the Minimal Information for Studies of Extracellular Vesicles (MISEV) guidelines (Vella et al., 2017; Welsh et al., 2024). Tunable Resisting Pulse sensing analysis (TRPS) is congruent with TEM results (Fig. 5B) and shows a peak size in the range 75–150 nm, consistent with the size of small EVs. The isolated small EV fraction demonstrated a high enrichment in all analyzed positive EV markers (CD63, CD9, ALG-2 interacting protein X, ALIX), except for one (syntenin-1), compared to corresponding cell homogenates (referred to as "cells"; Fig. 5C). Additionally, negative control markers, the endoplasmic reticulum protein calnexin (CNX) and Golgi apparatus protein GM-130, were depleted in the small EV fraction (Fig. 5C). These results indicate a high yield and the high purity of the small EV fraction. Fig. 5D demonstrates the cell–specific markers: neural cell adhesion molecule L1 (L1CAM), also known as cluster of differentiation molecule CD171 (predominantly neurons; ~140 kDa), CD11b (microglia; ~130 kDa), fragments of GLAST (astrocytes; ~60 kDa), and myelin oligodendrocyte glycoprotein (MOG) (oligodendrocytes; ~30 kDa),

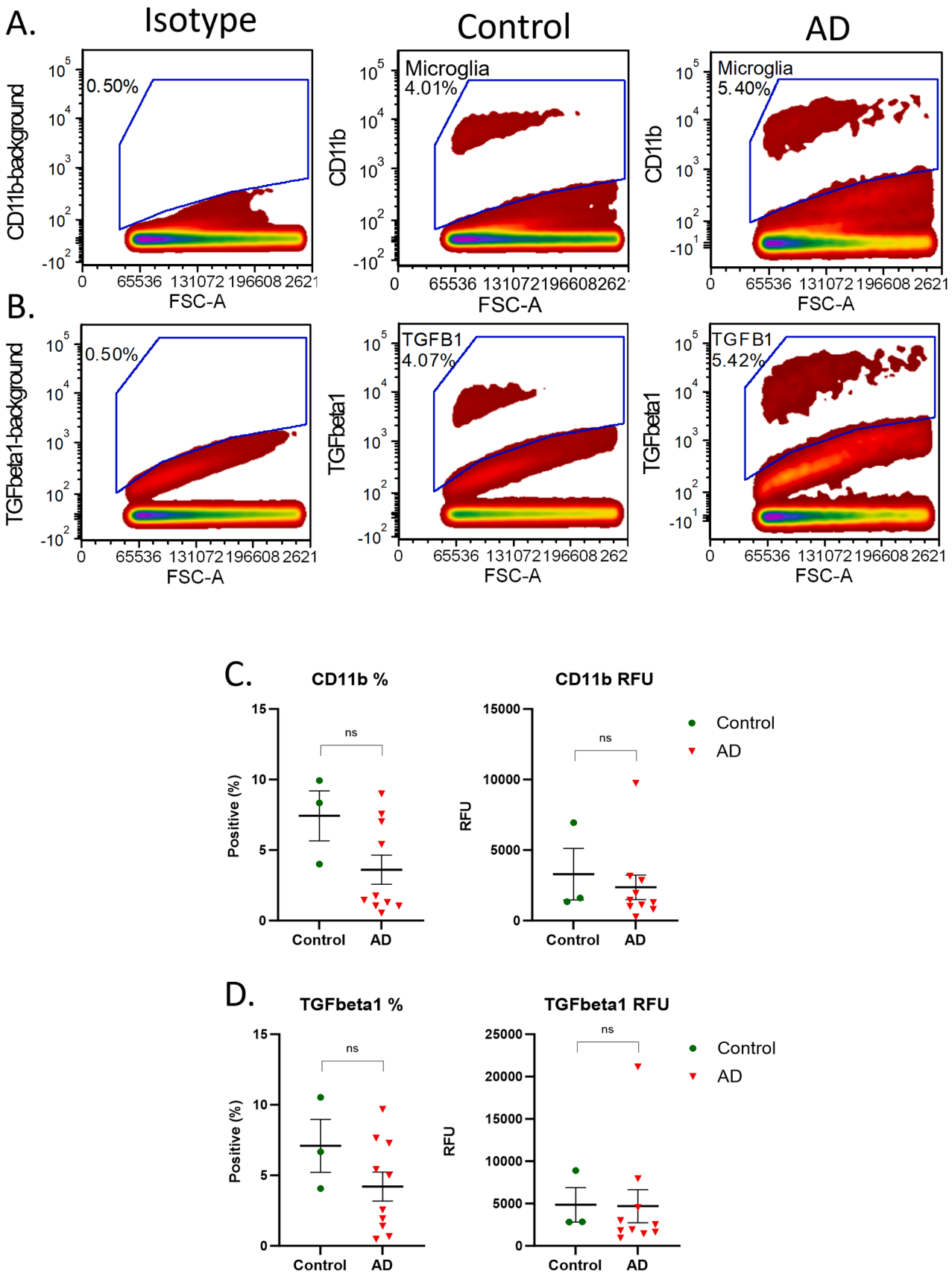

Fig. 4. CD11b-positive cell population in human cortex from control and late-stage AD cases. (A) CD11b and (B) TGFβ1 immunolabeling in the parietal cortex: isotype control (left), control brain (middle) and AD brain (right). (C) CD11b percent positive (left) and RFU (right) from the intact cell population in control and AD brains. (D) TGFβ1 % positive (left) and RFU (right) from the intact cell population in control and AD brains. n=3 for Control, n=10 for late-stage AD cases.

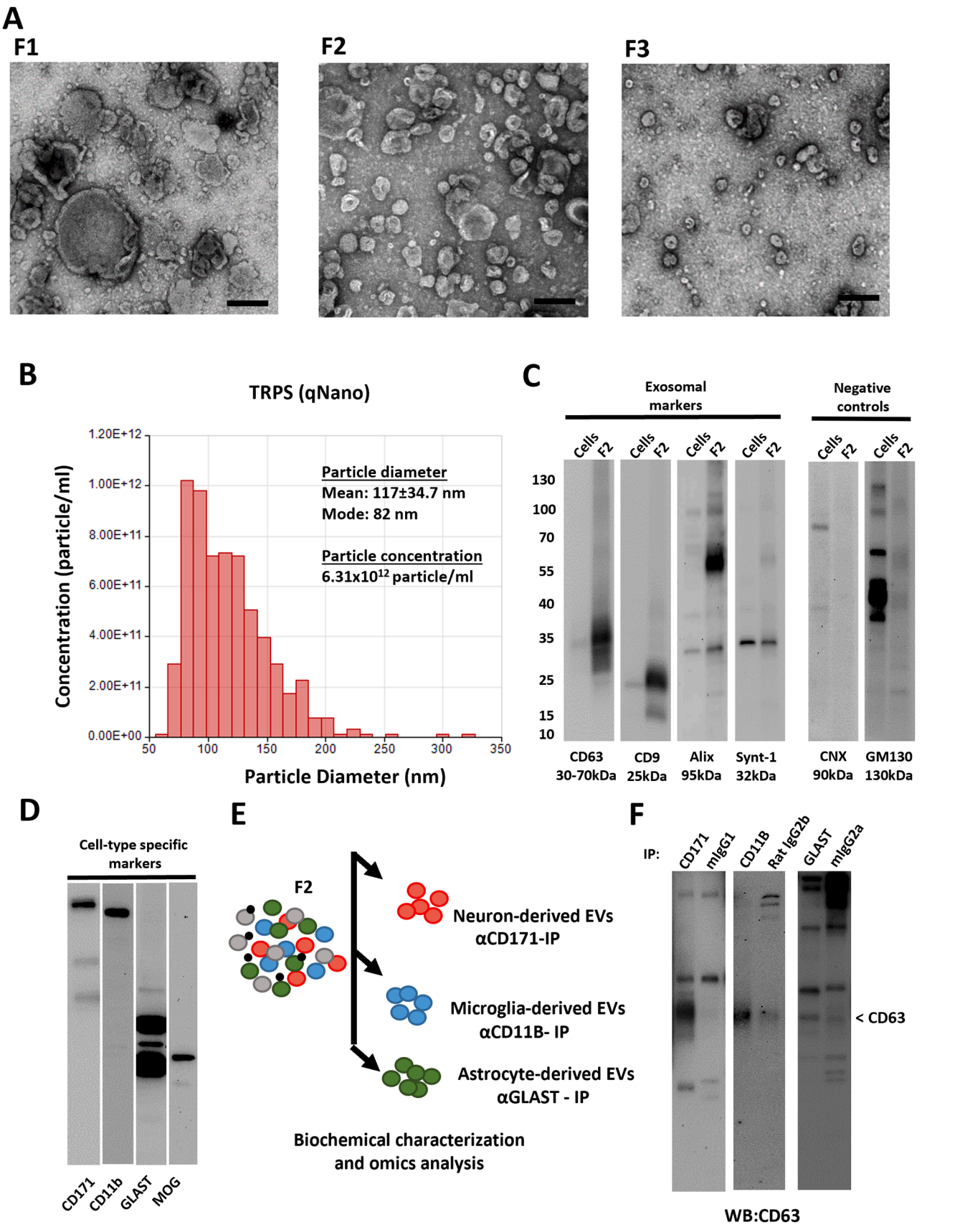

(caption on next page)

Fig. 5. Characterization of small EVs. (A) Transmission electron microscopy (TEM) of fractions F1 (left), F2 (center) and F3 (right). F2, small EV fraction, contained the highest number of vesicles in the size range from 30 to 200 nm, and was used for later analysis; bar is 100 nm. (B) Tunable Resisting Pulse sensing analysis (TRPS) using qNano Gold instrument shows mean particle diameter and concentration in small EV fraction, confirming TEM. (C) Western blots show enrichment of most of the analyzed positive control markers (CD63, CD9, and ALIX) except syntenin-1 compared to corresponded cell homogenates (cells), and depletion of negative control markers, GM130 and calnexin (CNX) in small EV fraction. (D) Cell-type specific markers: CD171/L1CAM (predominantly neurons), CD11b (microglia), GLAST (astrocytes), and MOG (oligodendrocytes) were detected in the F2 fraction. (E) Scheme of consecutive IP isolation of cell-specific brain EVs. (F) A representative image of immunoblot analysis of immunoprecipitation (IP) samples pull-down with antibodies against cell-type specific markers compared with corresponding isotype control antibodies (mIgG1, rat IgG2b, mIgG2a). Membrane was probed with the EV marker CD63.

confirming our ability to identify cell-type specific surface markers which could be used to isolate cell-specific small EVs. GLAST is known to be sensitive to papain (Kantzer et al., 2017), thus for consecutive immunoprecipitation of cell-specific small EVs we used trypsin-based dissociation of brain tissue. Fig. 5E shows a scheme of sequential isolation of neuronal (CD171-positive), microglial (CD11b-positive), and astrocytic (GLAST-positive) small EVs. Immunoblot analysis demonstrated the enrichment of EV marker CD63 in immunoprecipitated cell-specific EVs when compared to corresponding isotype controls (Fig. 5F). Note that the neuronal specificity of CD171 (L1CAM), a protein generally regarded as a marker of neurons, has been questioned as it is expressed in oligodendrocytes and cells outside of the brain (Hill, 2019). Therefore, potentially different neuronal markers or even a combination of markers may benefit the accuracy and yield of cell-specific EV isolation. Our isolation method provides a pathway for purification of cell-type specific small EVs and allows detailed biochemical and omics analysis as we recently published (Cohn et al., 2021).

4. Discussion

The present study demonstrates our ability to successfully isolate multiple different brain cell populations along with cell-specific small EVs from a single cryopreserved human AD sample. In most banks, the bulk of human postmortem tissue is either flash frozen at −80 °C, formalin fixed, or formalin fixed and paraffin-embedded for long term storage, in which the condition of DNA, RNA, and protein may be compromised, based on the agonal state, post-mortem delay, temperature of storage, and procedures of tissue preparation (Ferrer et al., 2008). More recently, cryopreservation has also been used for single cell RNA sequencing studies, in some studies with comparable gene expression results, although reduced cell yield and some cell damage was noted in one study (Denisenko et al., 2020; Ferrer et al., 2008; Guillaumet-Adkins et al., 2017). The advantage of human tissue over animal or *in vitro* studies are enormous and many useful results have been obtained, but the literature is clear that there is substantial variability across all studies of human postmortem brain, based on methodological details that include tissue and cell type, temperature and method of dissociation, and the analytic workflow (AlJanahi et al., 2018; Guillaumet-Adkins et al., 2017; Mattei et al., 2020). A number of labs routinely cryopreserve tissue with DMSO or sucrose solutions, primarily for studies of synaptosomes (resealed nerve terminals) (Biesemann et al., 2014; Fein et al., 2008; Gajera et al., 2019). Cryopreserved postmortem human synaptosomes can also be used for functional studies of synapses such as dopamine transport (Mash et al., 2002), glutamate and GABA release (Kuo and Dodd, 2011), tau release (Sokolow et al., 2015), and chemical LTP (Prieto et al., 2017). The successful use of cryopreservation in tissue culture and for functional synaptosomes highlights the degree to which membranes and proteins are preserved.

TGFβ has been considered a M2 phenotype marker with anti-inflammatory and protective properties (Jurga et al., 2020), sometimes considered 'homeostatic' (Krasemann et al., 2017). Historically, CD11b has been considered to label activated as well as resting microglia; more recent studies consider it part of the canonical or core transcriptional microglial signature (Patir et al., 2019). A recent RNA-seq study of a large population of postmortem human microglia showed ~80 % in clusters thought to represent 'homeostatic' microglia (Olah et al., 2020). Importantly, recent expert consensus cautions against labeling the activation state of glial cells based on transcriptomic studies or small groups of markers (Escartin et al., 2021). Therefore, we report only the size of the positive fraction (18–19 %) and the complete colocalization that we observe for CD11b with TGFβ in individual AD cortical microglia (Fig. 3C). TGFβ in its latent form is associated with the plasma membrane of microglia via leucine-rich repeat-containing protein 33 (LRRC33) (Qin et al., 2018), so its co-localization with CD11b is expected. In a small cohort study that included three control and ten AD cases, we didn't observe a significant difference in the percentage of CD11b- and TGFβ- positive cells and the relative fluorescent intensity in the positive cell populations (Fig. 4A-D). Our TGFβ results are in line with transcriptomic studies who found no change in TGFβ1 expression in AD patients compared to controls (Mathys et. al., 2019, Zhou et. al., 2020). It is important to mention that brain cells positive for CD11b may be macrophages entering from the periphery. In future experiments, we plan to further validate microglia by labeling with CD44 and CD169, specific markers not seen in microglia but expressed by activated, infiltrating monocytes (Bennett et al., 2016; Butovsky et al., 2012). A notable advantage of the present method is the ability to document the colocalization of key markers in individual cells in hypothesis-driven experiments.

Oligodendrocyte progenitor cells are resident cells of the adult parenchyma and have many functions beyond myelination that include maintenance of the blood brain barrier and releasing immune modulators (Akay et al., 2021). Mature oligodendrocytes are expected to label with both MBP and O4, but we see a majority of cells label with MBP only. The relatively low level of dual labeling may reflect a lower expression level of O4, and may also represent a loss of regenerative capacity in the late AD cortical sample (de Castro and Bribian, 2005). The method presented here offers a novel option to study this and other cell populations, such as endothelial cells, at the protein level.

Transcriptomic and histological studies (Mathys et al., 2019; Pelvig et al., 2008; Zhou et al., 2020) show cell type proportions that are 25–60 % neuronal, 5–20 % astrocytic, 5–10 % microglial, 30–44 % oligodendrocytic, with minor amounts (0–2 %) of endothelial cells and pericytes. Our data mostly correlate with these estimations obtained by the different methods, with around 70–90 % of total intact cells labeled by neuronal (~10 %; Fig. 2B), astrocytic (~ 30 %; Fig. 2C), microglial (~3–20 %; Fig. 2D and Fig. 3A), or OPC/oligodendrocytic (~30%; Fig. 2D and E) markers in AD parietal cortex. The reduced level of neurons observed by our method may be explained by their higher sensitivity to mechanical dissociation due to their specific morphology with extensive dendritic and axonal processes. The remining intact cells (approximately 10–30 % depending on the case) may be derived from the blood, blood vessels or blood-vessel associated areas of the brain parenchyma, such as T cells, endothelial cells, and pericytes. T cells themselves have also been found in the parenchyma of the brain (Su et al., 2023).

EV studies in AD to date have often focused on diagnostic potential and on pathogenic roles that include tau propagation (Abner et al., 2016; Asai et al., 2015; Bilousova et al., 2018; Fiandaca et al., 2015; Goetzl et al., 2018, 2016; Hamlett et al., 2017; Wang et al., 2017; Winston et al., 2016). Small EVs have been shown to be neuroprotective in ischemia by promoting angiogenesis in a number of studies (Tian et al., 2019; Xin et al., 2013); on the other hand, they may also promote inflammation in ischemia (Gao et al., 2020). Importantly, a growing

recent literature documents multiple instances of pathogenic as well as protective or repair roles for small EVs in multiple neurologic conditions; small EVs also have potential as drug delivery systems (Fan et al., 2022).

Differential ultracentrifugation has the disadvantage of being labor-intensive and requiring a large amount of starting material; at the same time, human cortical samples are generally at least a gram and often substantially larger. A combination of methods has been suggested to improve yield and purity (Stam et al., 2021); for example we have used immunoprecipitation to improve the yield of cell-specific EVs (Cohn et al., 2021). Along this line, it should also be noted that most available methods of EV isolation, including commercial precipitation kits, such as ExoQuick (System Biosciences) and Exoprep (HansaBioMed), can be applied to the original homogenate, or after the first three centrifugation steps to shorten the protocol. Given the use of bulk tissue, researchers must keep in mind that small EV isolation requires careful preparation and characterization to exclude synaptic and other contaminating vesicles in the isolates. Our recently published paper shows that the method of cell-specific EV purification described here allows the isolation of the high-purity fraction of small EVs of microglial origin from cryopreserved human brain tissue (Cohn et al., 2021). Moreover, multi-omics analysis revealed AD-associated signatures in the microglial EVs, demonstrating that the present method has merit for identifying novel EV-associated biomarkers. Nevertheless, using a single marker like CD11b may not be sufficient to isolate all the microglial small EVs and a combination of markers such as CD11b, P2ry12, and TMEM119 may be recommended for future studies. It is also important to mention that while classical neuronal markers like L1CAM or NCAM are highly expressed in neurons, they are not exclusively neuronal. For example, L1CAM is also expressed in oligodendrocytes and other cell types, including melanocytes and immune cells, for example T cells (Gomes and Witwer, 2022; Hill, 2019; Uhlen et al., 2015). Furthermore, epigenomic erosion and loss of cell type specificity in late AD stages (Xiong et al., 2023) may lead to ectopic expression of certain proteins, including classical cell-type markers. Therefore, all cell-type specific results should be interpreted with caution.

The present results demonstrate a procedure for the isolation of intact cells and small EVs from cryopreserved human postmortem samples, increasing the available options for use of banked tissue and maximizing the data yielded from each individual sample. Cryopreservation also provides a convenient option for animal brains under some circumstances, for example when treatments, large animal groups, or long procedures reduce the feasibility of immediate processing for animal tissues. Cryopreservation remains an option for isolation of cells prior to RNA sequencing studies (Guillaumet-Adkins et al., 2017; Wohnhaas et al., 2019); although we would highlight a great need for validation of these studies at the level of proteins. Given the huge potential for EVs in disease mechanisms, diagnostics and even therapeutics, there is an urgent need for understanding the basic science and for procedural options.

Funding

This work was supported by the National Institutes of Health [AG063767 to TB and KHG, AG051946 to KHG, AG18879 to CAM, and AG073377 to VJ]. The ARCs Foundation provided support for MM. Tissue was obtained from the AD Research Center Neuropathology Cores of USC [NIA P50 AG05142], UCLA [NIA P50 AG16570], and UC Irvine [NIA P30AG016573 and P30AG066519]. Flow cytometry was performed in the UCLA Jonsson Comprehensive Cancer Center (JCCC) and Center for AIDS Research Flow Cytometry Core Facility supported by NIH [CA16042 and AI28697], and by the JCCC, the UCLA AIDS Institute, the David Geffen School of Medicine and the Chancellor's Office at UCLA. Diagnosis, characterization and follow-up of 90+ Study subjects was supported by NIA [R01AG021055].

CRediT authorship contribution statement

Claudia Kawas: Writing – review & editing, Resources, Funding acquisition. **Maria Corrada:** Writing – review & editing, Resources, Funding acquisition. **Ryan Bohannan:** Investigation. **Karen Gylys:** Writing – original draft, Methodology, Funding acquisition, Conceptualization. **Mikhail Melnik:** Writing – original draft, Methodology, Investigation, Formal analysis, Conceptualization. **Tina Bilousova:** Writing – original draft, Methodology, Investigation, Funding acquisition, Formal analysis, Conceptualization. **Ricky Ma:** Investigation. **Emily Miyoshi:** Methodology, Investigation, Formal analysis. **Carol Miller:** Writing – review & editing, Resources, Funding acquisition. **Chad Caraway:** Investigation. **Varghese John:** Writing – review & editing, Methodology, Funding acquisition. **Jason Hinman:** Writing – review & editing, Methodology.

Declaration of Competing Interest

None.

Data Availability

No data was used for the research described in the article.

Acknowledgements

We thank Drs. Mari Perez-Rosendahl and Ronald C. Kim for UCI Neuropathology reports.

References

Abner, E.L., Jicha, G.A., Shaw, L.M., Trojanowski, J.Q., Goetzl, E.J., 2016. Plasma neuronal exosomal levels of Alzheimer's disease biomarkers in normal aging. Ann. Clin. Transl. Neurol. 3, 399–403.

Ahmad, F., Liu, P., 2020. Synaptosome as a tool in Alzheimer's disease research. Brain Res. 1746, 147009.

Akay, L.A., Effenberger, A.H., Tsai, L.H., 2021. Cell of all trades: oligodendrocyte precursor cells in synaptic, vascular, and immune function. Genes Dev. 35, 180–198.

AlJanahi, A.A., Danielsen, M., Dunbar, C.E., 2018. An introduction to the analysis of single-cell RNA-sequencing data. Mol. Ther. Methods Clin. Dev. 10, 189–196.

Asai, H., Ikezu, S., Tsunoda, S., Medalla, M., Luebke, J., Haydar, T., Wolozin, B., Butovsky, O., Kugler, S., Ikezu, T., 2015. Depletion of microglia and inhibition of exosome synthesis halt tau propagation. Nat. Neurosci. 18, 1584–1593.

Bennett, M.L., Bennett, F.C., Liddelow, S.A., Ajami, B., Zamanian, J.L., Fernhoff, N.B., Mulinyawe, S.B., Bohlen, C.J., Adil, A., Tucker, A., Weissman, I.L., Chang, E.F., Li, G., Grant, G.A., Hayden Gephart, M.G., Barres, B.A., 2016. New tools for studying microglia in the mouse and human CNS. Proc. Natl. Acad. Sci. USA 113, E1738–E1746.

Biesemann, C., Gronborg, M., Luquet, E., Wichert, S.P., Bernard, V., Bungers, S.R., Cooper, B., Varoqueaux, F., Li, L., Byrne, J.A., Urlaub, H., Jahn, O., Brose, N., Herzog, E., 2014. Proteomic screening of glutamatergic mouse brain synaptosomes isolated by fluorescence activated sorting. EMBO J. 33, 157–170.

Bilousova, T., Elias, C., Miyoshi, E., Alam, M.P., Zhu, C., Campagna, J., Vadivel, K., Jagodzinska, B., Gylys, K.H., John, V., 2018. Suppression of tau propagation using an inhibitor that targets the DK-switch of nSMase2. Biochem. Biophys. Res. Commun. 499, 751–757.

Bisht, K., Sharma, K.P., Lecours, C., Sanchez, M.G., El Hajj, H., Milior, G., Olmos-Alonso, A., Gomez-Nicola, D., Luheshi, G., Vallieres, L., Branchi, I., Maggi, L., Limatola, C., Butovsky, O., Tremblay, M.E., 2016. Dark microglia: a new phenotype predominantly associated with pathological states. Glia 64, 826–839.

Buss, L.F., Levi, J.E., Longatto-Filho, A., Cohen, D.D., Cury, L., Martins, T.R., Fuza, L.M., Villa, L.L., Eluf-Neto, J., 2021. Attendance for diagnostic colposcopy among high-risk human papillomavirus positive women in a Brazilian feasibility study. Int. J. Gynaecol. Obstet. 152, 72–77.

Butovsky, O., Jedrychowski, M.P., Moore, C.S., Cialic, R., Lanser, A.J., Gabriely, G., Koeglsperger, T., Dake, B., Wu, P.M., Doykan, C.E., Fanek, Z., Liu, L., Chen, Z., Rothstein, J.D., Ransohoff, R.M., Gygi, S.P., Antel, J.P., Weiner, H.L., 2014. Identification of a unique TGF-beta-dependent molecular and functional signature in microglia. Nat. Neurosci. 17, 131–143.

Butovsky, O., Siddiqui, S., Gabriely, G., Lanser, A.J., Dake, B., Murugaiyan, G., Doykan, C.E., Wu, P.M., Gali, R.R., Iyer, L.K., Lawson, R., Berry, J., Krichevsky, A.M., Cudkowicz, M.E., Weiner, H.L., 2012. Modulating inflammatory monocytes with a unique microRNA gene signature ameliorates murine ALS. J. Clin. Invest 122, 3063–3087.

de Castro, F., Bribian, A., 2005. The molecular orchestra of the migration of oligodendrocyte precursors during development. Brain Res. Brain Res. Rev. 49, 227–241.

Cohn, W., Melnik, M., Huang, C., Teter, B., Chandra, S., Zhu, C., McIntire, L.B., John, V., Gylys, K.H., Bilousova, T., 2021. Multi-omics analysis of microglial extracellular vesicles from human Alzheimer's disease brain tissue reveals disease-associated signatures. Front. Pharm. 12, 766082.

Denisenko, E., Guo, B.B., Jones, M., Hou, R., de Kock, L., Lassmann, T., Poppe, D., Clement, O., Simmons, R.K., Lister, R., Forrest, A.R.R., 2020. Systematic assessment of tissue dissociation and storage biases in single-cell and single-nucleus RNA-seq workflows. Genome Biol. 21, 130.

Dodd, P.R., Hardy, J.A., Baig, E.B., Kidd, A.M., Bird, E.D., Watson, W.E., Johnston, G.A., 1986. Optimization of freezing, storage, and thawing conditions for the preparation of metabolically active synaptosomes from frozen rat and human brain. Neurochem. Pathol. 4, 177–198.

Escartin, C., Galea, E., Lakatos, A., O'Callaghan, J.P., Petzold, G.C., Serrano-Pozo, A., Steinhauser, C., Volterra, A., Carmignoto, G., Agarwal, A., Allen, N.J., Araque, A., Barbeito, L., Barzilai, A., Bergles DE, Bonvento, G., Butt, A.M., Chen, W.T., Cohen-Salmon, M., Cunningham, C., Deneen, B., De Strooper, B., Diaz-Castro, B., Farina, C., Freeman, M., Gallo, V., Goldman, J.E., Goldman, S.A., Gotz, M., Gutierrez, A., Haydon, P.G., Heiland, D.H., Hol, E.M., Holt, M.G., Iino, M., Kastanenka, K.V., Kettenmann, H., Khakh, B.S., Koizumi, S., Lee, C.J., Liddelow, S.A., MacVicar, B.A., Magistretti, P., Messing, A., Mishra, A., Molofsky, A.V., Murai, K.K., Norris, C.M., Okada, S., Oliet, S.H.R., Oliveira, J.F., Panatier, A., Parpura, V., Pekna, M., Pekny, M., Pellerin, L., Perea, G., Perez-Nievas, B.G., Pfrieger, F.W., Poskanzer, K.E., Quintana, F.J., Ransohoff, R.M., Riquelme-Perez, M., Robel, S., Rose, C.R., Rothstein, J.D., Rouach, N., Rowitch, D.H., Semyanov, A., Sirko, S., Sontheimer, H., Swanson, R.A., Vitorica, J., Wanner, I.B., Wood, L.B., Wu, J., Zheng, B., Zimmer, E. R., Zorec, R., Sofroniew, M.V., Verkhratsky, A., 2021. Reactive astrocyte nomenclature, definitions, and future directions. Nat. Neurosci. 24, 312–325.

Fan, Y., Chen, Z., Zhang, M., 2022. Role of exosomes in the pathogenesis, diagnosis, and treatment of central nervous system diseases. J. Transl. Med 20, 291.

Fein, J.A., Sokolow, S., Miller, C.A., Vinters, H.V., Yang, F., Cole, G.M., Gylys, K.H., 2008. Co-localization of amyloid beta and tau pathology in Alzheimer's disease synaptosomes. Am. J. Pathol. 172, 1683–1692.

Fernandes, A., Ribeiro, A.R., Monteiro, M., Garcia, G., Vaz, A.R., Brites, D., 2018. Secretome from SH-SY5Y APPSwe cells trigger time-dependent CHME3 microglia activation phenotypes, ultimately leading to miR-21 exosome shuttling. Biochimie 155, 67–82.

Ferrer, I., Martinez, A., Boluda, S., Parchi, P., Barrachina, M., 2008. Brain banks: benefits, limitations and cautions concerning the use of post-mortem brain tissue for molecular studies. Cell Tissue Bank 9, 181–194.

Fiandaca, M.S., Kapogiannis, D., Mapstone, M., Boxer, A., Eitan, E., Schwartz, J.B., Abner, E.L., Petersen, R.C., Federoff, H.J., Miller, B.L., Goetzl, E.J., 2015. Identification of preclinical Alzheimer's disease by a profile of pathogenic proteins in neurally derived blood exosomes: a case-control study. Alzheimer'S. Dement.: J. Alzheimer'S. Assoc. 11, 600-7.e1.

Gajera, C.R., Fernandez, R., Postupna, N., Montine, K.S., Fox, E.J., Tebaykin, D., Angelo, M., Bendall, S.C., Keene, C.D., Montine, T.J., 2019. Mass synaptometry: high-dimensional multi parametric assay for single synapses. J. Neurosci. Methods 312, 73–83.

Gao, G., Li, C., Zhu, J., Wang, Y., Huang, Y., Zhao, S., Sheng, S., Song, Y., Ji, C., Li, C., Yang, X., Ye, L., Qi, X., Zhang, Y., Xia, X., Zheng, J.C., 2020. Glutaminase 1 regulates neuroinflammation after cerebral ischemia through enhancing microglial activation and pro-inflammatory exosome release. Front Immunol. 11, 161.

Gao, G., Zhao, S., Xia, X., Li, C., Li, C., Ji, C., Sheng, S., Tang, Y., Zhu, J., Wang, Y., Huang, Y., Zheng, J.C., 2019. Glutaminase C regulates microglial activation and pro-inflammatory exosome release: relevance to the pathogenesis of Alzheimer's disease. Front. Cell Neurosci. 13, 264.

Goetzl, E.J., Abner, E.L., Jicha, G.A., Kapogiannis, D., Schwartz, J.B., 2018. Declining levels of functionally specialized synaptic proteins in plasma neuronal exosomes with progression of Alzheimer's disease. FASEB J. 32, 888–893.

Goetzl, E.J., Kapogiannis, D., Schwartz, J.B., Lobach, I.V., Goetzl, L., Abner, E.L., Jicha, G.A., Karydas, A.M., Boxer, A., Miller, B.L., 2016. Decreased synaptic proteins in neuronal exosomes of frontotemporal dementia and Alzheimer's disease. FASEB J. 30, 4141–4148.

Gomes, D.E., Witwer, K.W., 2022. L1CAM-associated extracellular vesicles: a systematic review of nomenclature, sources, separation, and characterization. J. Extra Biol. 1.

Grubman, A., Choo, X.Y., Chew, G., Ouyang, J.F., Sun, G., Croft, N.P., Rossello, F.J., Simmons, R., Buckberry, S., Landin, D.V., Pflueger, J., Vandekolk, T.H., Abay, Z., Zhou, Y., Liu, X., Chen, J., Larcombe, M., Haynes, J.M., McLean, C., Williams, S., Chai, S.Y., Wilson, T., Lister, R., Pouton, C.W., Purcell, A.W., Rackham, O.J.L., Petretto, E., Polo, J.M., 2021. Transcriptional signature in microglia associated with Abeta plaque phagocytosis. Nat. Commun. 12, 3015.

Guillaumet-Adkins, A., Rodriguez-Esteban, G., Mereu, E., Mendez-Lago, M., Jaitin, D.A., Villanueva, A., Vidal, A., Martinez-Marti, A., Felip, E., Vivancos, A., Keren-Shaul, H., Heath, S., Gut, M., Amit, I., Gut, I., Heyn, H., 2017. Single-cell transcriptome conservation in cryopreserved cells and tissues. Genome Biol. 18, 45.

Guix, F.X., Corbett, G.T., Cha, D.J., Mustapic, M., Liu, W., Mengel, D., Chen, Z., Aikawa, E., Young-Pearse, T., Kapogiannis, D., Selkoe, D.J., Walsh, D.M., 2018. Detection of aggregation-competent tau in neuron-derived extracellular vesicles. Int. J. Mol. Sci. 19.

Gylys, K.H., Bilousova, T., 2017. Flow cytometry analysis and quantitative characterization of tau in synaptosomes from Alzheimer's disease brains. Methods Mol. Biol. 1523, 273–284.

Hamlett, E.D., Goetzl, E.J., Ledreux, A., Vasilevko, V., Boger, H.A., LaRosa, A., Clark, D., Carroll, S.L., Carmona-Iragui, M., Fortea, J., Mufson, E.J., Sabbagh, M., Mohammed, A.H., Hartley, D., Doran, E., Lott, I.T., Granholm, A.C., 2017. Neuronal exosomes reveal Alzheimer's disease biomarkers in down syndrome. Alzheimer. Dement. J. Alzheimer. Assoc. 13, 541–549.

Hasel, P., Rose, I.V.L., Sadick, J.S., Kim, R.D., Liddelow, S.A., 2021. Neuroinflammatory astrocyte subtypes in the mouse brain. Nat. Neurosci. 24, 1475–1487.

Heinzelman, P., Bilousova, T., Campagna, J., John, V., 2016. Nanoscale extracellular vesicle analysis in Alzheimer's disease diagnosis and therapy. Int J. Alzheimers Dis. 2016, 8053139.

Hill, A.F., 2019. Extracellular vesicles and neurodegenerative diseases. J. Neurosci. 39, 9269–9273.

Hussain, R.Z., Miller-Little, W.A., Doelger, R., Cutter, G.R., Loof, N., Cravens, P.D., Stuve, O., 2018. Defining standard enzymatic dissociation methods for individual brains and spinal cords in EAE. Neurol. Neuroimmunol. Neuroinflamm. 5, e437.

Jurga, A.M., Paleczna, M., Kuter, K.Z., 2020. Overview of general and discriminating markers of differential microglia phenotypes. Front Cell Neurosci. 14, 198.

Kantzer, C.G., Boutin, C., Herzig, I.D., Wittwer, C., Reiss, S., Tiveron, M.C., Drewes, J., Rockel, T.D., Ohlig, S., Ninkovic, J., Cremer, H., Pennartz, S., Jungblut, M., Bosio, A., 2017. Anti-ACSA-2 defines a novel monoclonal antibody for prospective isolation of living neonatal and adult astrocytes. Glia 65, 990–1004.

Kaufman, S.K., Thomas, T.L., Del Tredici, K., Braak, H., Diamond, M.I., 2017. Characterization of tau prion seeding activity and strains from formaldehyde-fixed tissue. Acta Neuropathol. Commun. 5, 41.

Keren-Shaul, H., Spinrad, A., Weiner, A., Matcovitch-Natan, O., Dvir-Szternfeld, R., Ulland, T.K., David, E., Baruch, K., Lara-Astaiso, D., Toth, B., Itzkovitz, S., Colonna, M., Schwartz, M., Amit, I., 2017. A unique microglia type associated with restricting development of Alzheimer's disease. Cell 169, 1276–1290 e17.

Krasemann, S., Madore, C., Cialic, R., Baufeld, C., Calcagno, N., El Fatimy, R., Beckers, L., O'Loughlin, E., Xu, Y., Fanek, Z., Greco, D.J., Smith, S.T., Tweet, G., Humulock, Z., Zrzavy, T., Conde-Sanroman, P., Gacias, M., Weng, Z., Chen, H., Tjon, E., Mazaheri, F., Hartmann, K., Madi, A., Ulrich, J.D., Glatzel, M., Worthmann, A., Heeren, J., Budnik, B., Lemere, C., Ikezu, T., Heppner, F.L., Litvak, V., Holtzman, D. M., Lassmann, H., Weiner, H.L., Ochando, J., Haass, C., Butovsky, O., 2017. The TREM2-APOE pathway drives the transcriptional phenotype of dysfunctional microglia in neurodegenerative diseases. Immunity 47, 566–581 e9.

Kuo, S.W., Dodd, P.R., 2011. Electrically evoked synaptosomal amino acid transmitter release in human brain in alcohol misuse. Neuro-Signals 19, 117–127.

Liddelow, S.A., Guttenplan, K.A., Clarke, L.E., Bennett, F.C., Bohlen, C.J., Schirmer, L., Bennett, M.L., Munch, A.E., Chung, W.S., Peterson, T.C., Wilton, D.K., Frouin, A., Napier, B.A., Panicker, N., Kumar, M., Buckwalter, M.S., Rowitch, D.H., Dawson, V. L., Dawson, T.M., Stevens, B., Barres, B.A., 2017. Neurotoxic reactive astrocytes are induced by activated microglia. Nature 541, 481–487.

Mash, D.C., Pablo, J., Ouyang, Q., Hearn, W.L., Izenwasser, S., 2002. Dopamine transport function is elevated in cocaine users. J. Neurochem 81, 292–300.

Mathys, H., Davila-Velderrain, J., Peng, Z., Gao, F., Mohammadi, S., Young, J.Z., Menon, M., He, L., Abdurrob, F., Jiang, X., Martorell, A.J., Ransohoff, R.M., Hafler, B.P., Bennett, D.A., Kellis, M., Tsai, L.H., 2019. Single-cell transcriptomic analysis of Alzheimer's disease. Nature 570, 332–337.

Mattei, D., Ivanov, A., van Oostrum, M., Pantelyushin, S., Richetto, J., Mueller, F., Beffinger, M., Schellhammer, L., Vom Berg, J., Wollscheid, B., Beule, D., Paolicelli, R.C., Meyer, U., 2020. Enzymatic dissociation induces transcriptional and proteotype bias in brain cell populations. Int J. Mol. Sci. 21.

de la Monte, S.M., Grammas, P., 2019. In: Wisniewski, T. (Ed.), Insulin Resistance and Oligodendrocyte/Microvascular Endothelial Cell Dysfunction as Mediators of White Matter Degeneration in Alzheimer's Disease. Alzheimer's Disease, Brisbane (AU).

Olah, M., Menon, V., Habib, N., Taga, M.F., Ma, Y., Yung, C.J., Cimpean, M., Khairallah, A., Coronas-Samano, G., Sankowski, R., Grun, D., Kroshilina, A.A., Dionne, D., Sarkis, R.A., Cosgrove, G.R., Helgager, J., Golden, J.A., Pennell, P.B., Prinz, M., Vonsattel, J.P.G., Teich, A.F., Schneider, J.A., Bennett, D.A., Regev, A., Elyaman, W., Bradshaw, E.M., De Jager, P.L., 2020. Single cell RNA sequencing of human microglia uncovers a subset associated with Alzheimer's disease. Nat. Commun. 11, 6129.

Palmero, E., Palmero, S., Murrell, W., 2016. Brain tissue banking for stem cells for our future. Sci. Rep. 6, 39394.

Patir, A., Shih, B., McColl, B.W., Freeman, T.C., 2019. A core transcriptional signature of human microglia: Derivation and utility in describing region-dependent alterations associated with Alzheimer's disease. Glia 67, 1240–1253.

Pelvig, D.P., Pakkenberg, H., Stark, A.K., Pakkenberg, B., 2008. Neocortical glial cell numbers in human brains. Neurobiol. Aging 29, 1754–1762.

Polanco, J.C., Scicluna, B.J., Hill, A.F., Gotz, J., 2016. Extracellular vesicles isolated from the brains of rTg4510 mice seed tau protein aggregation in a threshold-dependent manner. J. Biol. Chem. 291, 12445–12466.

Prieto, G.A., Trieu, B.H., Dang, C.T., Bilousova, T., Gylys, K.H., Berchtold, N.C., Lynch, G., Cotman, C.W., 2017. Pharmacological rescue of long-term potentiation in Alzheimer diseased synapses. J. Neurosci. 37, 1197–1212.

Qin, Y., Garrison, B.S., Ma, W., Wang, R., Jiang, A., Li, J., Mistry, M., Bronson, R.T., Santoro, D., Franco, C., Robinton, D.A., Stevens, B., Rossi, D.J., Lu, C., Springer, T.A., 2018. A Milieu Molecule for TGF-beta required for microglia function in the nervous system. Cell 174, 156–171 e16.

Rastogi, S., Sharma, V., Bharti, P.S., Rani, K., Modi, G.P., Nikolajeff, F., Kumar, S., 2021. The Evolving landscape of exosomes in neurodegenerative diseases: exosomes characteristics and a promising role in early diagnosis. Int J. Mol. Sci. 22.

Sadick, J.S., O'Dea, M.R., Hasel, P., Dykstra, T., Faustin, A., Liddelow, S.A., 2022. Astrocytes and oligodendrocytes undergo subtype-specific transcriptional changes in Alzheimer's disease. Neuron 110, 1788–1805 e10.

Sokolow, S., Henkins, K.M., Bilousova, T., Gonzalez, B., Vinters, H.V., Miller, C.A., Cornwell, L., Poon, W.W., Gylys, K.H., 2015. Pre-synaptic C-terminal truncated tau is released from cortical synapses in Alzheimer's disease. J. Neurochem 133, 368–379.

Spaas, J., van Veggel, L., Schepers, M., Tiane, A., van Horssen, J., Wilson 3rd, D.M., Moya, P.R., Piccart, E., Hellings, N., Eijnde, B.O., Derave, W., Schreiber, R., Vanmierlo, T., 2021. Oxidative stress and impaired oligodendrocyte precursor cell differentiation in neurological disorders. Cell Mol. Life Sci.

Srinivasan, K., Friedman, B.A., Larson, J.L., Lauffer, B.E., Goldstein, L.D., Appling, L.L., Borneo, J., Poon, C., Ho, T., Cai, F., Steiner, P., van der Brug, M.P., Modrusan, Z., Kaminker, J.S., Hansen, D.V., 2016. Untangling the brain's neuroinflammatory and neurodegenerative transcriptional responses. Nat. Commun. 7, 11295.

Stam, J., Bartel, S., Bischoff, R., Wolters, J.C., 2021. Isolation of extracellular vesicles with combined enrichment methods. J. Chromatogr. B Anal. Technol. Biomed. Life Sci. 1169, 122604.

Su, W., Saravia, J., Risch, I., Rankin, S., Guy, C., Chapman, N.M., Shi, H., Sun, Y., Kc, A., Li, W., Huang, H., Lim, S.A., Hu, H., Wang, Y., Liu, D., Jiao, Y., Chen, P.C., Soliman, H., Yan, K.K., Zhang, J., Vogel, P., Liu, X., Serrano, G.E., Beach, T.G., Yu, J., Peng, J., Chi, H., 2023. CXCR6 orchestrates brain CD8(+) T cell residency and limits mouse Alzheimer's disease pathology. Nat. Immunol. 24, 1735–1747.

Thery, C., Amigorena, S., Raposo, G., Clayton, A., 2006. Isolation and characterization of exosomes from cell culture supernatants and biological fluids. Curr. Protoc. Cell Biol. Chapter 3: Unit 3 22.

Tian, Y., Zhu, P., Liu, S., Jin, Z., Li, D., Zhao, H., Zhu, X., Shu, C., Yan, D., Dong, Z., 2019. IL-4-polarized BV2 microglia cells promote angiogenesis by secreting exosomes. Adv. Clin. Exp. Med 28, 421–430.

Uhlen, M., Fagerberg, L., Hallstrom, B.M., Lindskog, C., Oksvold, P., Mardinoglu, A., Sivertsson, A., Kampf, C., Sjostedt, E., Asplund, A., Olsson, I., Edlund, K., Lundberg, E., Navani, S., Szigyarto, C.A., Odeberg, J., Djureinovic, D., Takanen, J.O., Hober, S., Alm, T., Edqvist, P.H., Berling, H., Tegel, H., Mulder, J., Rockberg, J., Nilsson, P., Schwenk, J.M., Hamsten, M., von Feilitzen, K., Forsberg, M., Persson, L., Johansson, F., Zwahlen, M., von Heijne, G., Nielsen, J., Ponten, F., 2015. Proteomics. tissue-based map of the human proteome. Science 347, 1260419.

Vella, L.J., Scicluna, B.J., Cheng, L., Bawden, E.G., Masters, C.L., Ang, C.S., Willamson, N., McLean, C., Barnham, K.J., Hill, A.F., 2017. A rigorous method to enrich for exosomes from brain tissue. J. Extra Vesicles 6, 1348885.

Wang, Y., Balaji, V., Kaniyappan, S., Kruger, L., Irsen, S., Tepper, K., Chandupatla, R., Maetzler, W., Schneider, A., Mandelkow, E., Mandelkow, E.M., 2017. The release and trans-synaptic transmission of Tau via exosomes. Mol. Neurodegener. 12, 5.

Welsh, J.A., Goberdhan, D.C.I., O'Driscoll, L., Buzas, E.I., Blenkiron, C., Bussolati, B., Cai, H., Di Vizio, D., Driedonks, T.A.P., Erdbrugger, U., Falcon-Perez, J.M., Fu, Q.L., Hill, A.F., Lenassi, M., Lim, S.K., Mahoney, M.G., Mohanty, S., Moller, A., Nieuwland, R., Ochiya, T., Sahoo, S., Torrecilhas, A.C., Zheng, L., Zijlstra, A., Abuelreich, S., Bagabas, R., Bergese, P., Bridges, E.M., Brucale, M., Burger, D., Carney, R.P., Cocucci, E., Crescitelli, R., Hanser, E., Harris, A.L., Haughey, N.J., Hendrix, A., Ivanov, A.R., Jovanovic-Talisman, T., Kruh-Garcia, N.A., Ku'ulei-Lyn Faustino, V., Kyburz, D., Lasser, C., Lennon, K.M., Lotvall, J., Maddox, A.L., Martens-Uzunova, E.S., Mizenko, R.R., Newman, L.A., Ridolfi, A., Rohde, E., Rojalin, T., Rowland, A., Saftics, A., Sandau, U.S., Saugstad, J.A., Shekari, F., Swift, S., Ter-Ovanesyan, D., Tosar, J.P., Useckaite, Z., Valle, F., Varga, Z., van der Pol, E., van Herwijnen, M.J.C., Wauben, M.H.M., Wehman, A.M., Williams, S., Zendrini, A., Zimmerman, A.J., Consortium, M., Thery, C., Witwer, K.W., 2024. Minimal information for studies of extracellular vesicles (MISEV2023): from basic to advanced approaches. J. Extra Vesicles 13, e12404.

Winston, C.N., Goetzl, E.J., Akers, J.C., Carter, B.S., Rockenstein, E.M., Galasko, D., Masliah, E., Rissman, R.A., 2016. Prediction of conversion from mild cognitive impairment to dementia with neuronally derived blood exosome protein profile. Alzheimers Dement 3, 63–72.

Wohnhaas, C.T., Leparc, G.G., Fernandez-Albert, F., Kind, D., Gantner, F., Viollet, C., Hildebrandt, T., Baum, P., 2019. DMSO cryopreservation is the method of choice to preserve cells for droplet-based single-cell RNA sequencing. Sci. Rep. 9, 10699.

Wylot, B., Konarzewska, K., Bugajski, L., Piwocka, K., Zawadzka, M., 2015. Isolation of vascular endothelial cells from intact and injured murine brain cortex-technical issues and pitfalls in FACS analysis of the nervous tissue. Cytom. A 87, 908–920.

Xin, H., Li, Y., Cui, Y., Yang, J.J., Zhang, Z.G., Chopp, M., 2013. Systemic administration of exosomes released from mesenchymal stromal cells promote functional recovery and neurovascular plasticity after stroke in rats. J. Cereb. Blood Flow. Metab. 33, 1711–1715.

Xiong, X., James, B.T., Boix, C.A., Park, Y.P., Galani, K., Victor, M.B., Sun, N., Hou, L., Ho, L.L., Mantero, J., Scannail, A.N., Dileep, V., Dong, W., Mathys, H., Bennett, D.A., Tsai, L.H., Kellis, M., 2023. Epigenomic dissection of Alzheimer's disease pinpoints causal variants and reveals epigenome erosion. Cell 186, 4422–4437 e21.

Zhou, Y., Song, W.M., Andhey, P.S., Swain, A., Levy, T., Miller, K.R., Poliani, P.L., Cominelli, M., Grover, S., Gilfillan, S., Cella, M., Ulland, T.K., Zaitsev, K., Miyashita, A., Ikeuchi, T., Sainouchi, M., Kakita, A., Bennett, D.A., Schneider, J.A., Nichols, M.R., Beausoleil, S.A., Ulrich, J.D., Holtzman, D.M., Artyomov, M.N., Colonna, M., 2020. Human and mouse single-nucleus transcriptomics reveal TREM2-dependent and TREM2-independent cellular responses in Alzheimer's disease. Nat. Med. 26, 131–142.